aerospace

MDPI

Article

Comprehensive Assessment of BDS Precise Orbit and Clock Products from IGS MGEX Analysis Centers

Jing Qiao [1,2], Shuping Liu [1] and Haibo Ge [1,*]

[1] College of Surveying and Geo-Informatics, Tongji University, Shanghai 200092, China; jingqiao@tongji.edu.cn (J.Q.); 2533584@tongji.edu.cn (S.L.)
[2] Shanghai Key Laboratory of Space Navigation and Positioning Techniques, Shanghai Astronomical Observatory, Chinese Academy of Sciences, Shanghai 200030, China
* Correspondence: haibo_ge@tongji.edu.cn

Abstract

High-quality precise orbit and clock products are essential for high-precision positioning and space-geodetic applications, yet substantial quality differences are observed across orbit types and satellite products. The BeiDou Navigation Satellite System (BDS) precise orbit and clock products from 2025, provided by four analysis centers (ACs) of the International GNSS Service (IGS) Multi-GNSS Experiment (MGEX), are assessed using inter-center comparisons, Satellite Laser Ranging (SLR) validation, Allan deviation (ADEV) analysis, and static precise point positioning (PPP). For BDS-3 medium Earth orbit (MEO) satellites, the root mean square (RMS) values of three-dimensional (3D) orbit differences and clock residuals are 4.10–5.92 cm and 0.08–0.16 ns (2.4–4.8 cm in equivalent range), respectively. These values are 38.3–59.9% and 15.8–50.0% lower than those for BDS-2 MEO satellites. Inclined geosynchronous orbit (IGSO) satellite products exhibit markedly larger inter-center differences, with BDS-3 orbit-difference and clock-residual RMS values reaching up to 19.99 cm and 0.52 ns (15.6 cm in equivalent range), respectively. SLR validation gives group-level mean residuals of 3.58–5.61 cm for BDS-3 CAST satellites and −3.00 to −0.64 cm for SECM satellites, with standard deviations of 3.22–4.45 cm and 2.15–3.01 cm, respectively. Solar-geometry-dependent residual variations are observed for satellites with space vehicle numbers (SVNs) C215 and C223. Static PPP yields 3D RMS values of coordinate differences relative to the IGS weekly reference coordinates ranging from 1.82 to 4.72 cm across the four ACs. Adding IGSO satellites improves satellite visibility and observation geometry but does not consistently improve coordinate accuracy. Overall, BDS-3 MEO products demonstrate high inter-center consistency, whereas IGSO satellites and several anomalous spacecraft remain the primary limitations to further product refinement.

Keywords: BeiDou Navigation Satellite System; MGEX precise products; Satellite Laser Ranging; Allan deviation; inclined geosynchronous orbit; precise point positioning

Check for updates

Academic Editor: Stefano Silvestrini

Received: 8 September 2026
Revised: 10 November 2026
Accepted: 10 November 2026
Published: 18 November 2026

Copyright: © 2026 by the authors. Licensee MDPI, Basel, Switzerland. This article is an open access article distributed under the terms and conditions of the Creative Commons Attribution (CC BY) license.

1. Introduction

The BeiDou Navigation Satellite System (BDS) has developed from the regional BDS-2 system into the globally operational BDS-3 system [1]. BDS is one of the four global navigation satellite systems (GNSS), alongside the Global Positioning System (GPS), the Global Navigation Satellite System (GLONASS), and Galileo [2]. High-quality precise orbit and clock products are essential for precise point positioning, time synchronization, terrestrial reference frame maintenance, and other space-geodetic applications [3]. With the continued development of BDS, several analysis centers (ACs) participating in the

International GNSS Service (IGS) Multi-GNSS Experiment (MGEX) now routinely provide precise BDS orbit and clock products [4]. However, these centers use different tracking networks, dynamical models, and parameter estimation strategies, resulting in differences among their products [5]. Continued assessment of BDS precise orbit and clock products is therefore needed as the constellation status and processing strategies evolve.

Early assessments of MGEX products mainly relied on inter-center orbit and clock comparisons, Satellite Laser Ranging (SLR) validation, and precise point positioning (PPP). Using two years of MGEX data, Guo et al. [6] evaluated Galileo, BDS, and Quasi-Zenith Satellite System products and identified differences among constellations, orbit types, and ACs. Steigenberger and Montenbruck [5] subsequently documented the overall improvement in MGEX orbit and clock consistency as the underlying models evolved. Li et al. [7] analyzed the orbit, clock, SLR, and PPP performance of products available since 2018, whereas Shen et al. [8] compared BDS-3 orbit, clock, and PPP performance across ACs. Gu et al. [9] compared BDS-2 and BDS-3 satellite clocks using more than one year of precise clock products and examined their effects on PPP. Geng et al. [10] further investigated clock offsets, periodic signals, and frequency stability for the complete BDS-3 constellation. Collectively, these studies have established a comprehensive evaluation framework and revealed differences between BDS-2 and BDS-3, among orbit types and satellites, and across ACs.

As the BDS-3 constellation and external tracking capabilities have improved, research has expanded beyond overall product performance to full-constellation behavior, satellite-specific anomalies, and dynamical modeling. Steigenberger et al. [11] evaluated BDS-3 products from five MGEX ACs using product comparisons, SLR validation, clock-stability analysis, and PPP. They reported BDS-3 medium Earth orbit (MEO) consistency of 4–8 cm and SLR residual root mean square (RMS) values of 3–9 cm. They also identified systematic clock variations related to the Sun elevation angle above the orbital plane (β). Studies have shown that improved a priori or empirical solar radiation pressure (SRP) models can reduce solar-geometry-related errors in BDS-3 orbits [12,13]. After the International Laser Ranging Service (ILRS) expanded tracking to 24 BDS-3 MEO satellites in 2023, Zajdel et al. [14] reported marked differences among individual satellites. SLR residual standard deviations were approximately 19–20 mm for 14 satellites but exceeded 100 mm for eight others. For space vehicle numbers (SVNs) C223 and C222, Xie et al. [15] reported anomalous SLR residuals at large $|\beta|$ and identified payload configuration and SRP-model suitability as possible factors. Their combined physical and empirical SRP model reduced the corresponding residuals.

Although previous studies have established a framework combining orbit comparisons, SLR validation, clock-stability analysis, and PPP, much of the available evidence is based on earlier products or relatively short analysis periods. Since product generation strategies of ACs, the BDS constellation, and SLR tracking coverage continue to evolve, previous findings may not represent current product performance. A multi-level assessment of recently released products is therefore needed to characterize orbit consistency, external orbit quality, clock consistency, apparent clock stability, and user-domain positioning performance. Such an assessment can help users select products according to their applications and quality metrics of interest. It can also support anomaly screening, weighting strategies, and quality control for future combined BDS products. Examining the solar-geometry-related behavior of anomalous satellites may also reveal limitations in current orbit and clock processing. These findings can guide improvements in attitude, non-gravitational-force, and satellite-specific modeling.

In this study, the 2025 BDS precise orbit and clock products from four MGEX ACs are assessed using a multidimensional framework. Relative orbit consistency and external orbit

quality are evaluated through inter-center orbit comparisons and SLR validation, respectively. Clock consistency and apparent clock stability are assessed using clock comparisons and ADEV derived from precise clock products. The results are examined by BDS system, orbit type, manufacturer, and individual satellite. For selected anomalous satellites, the relationship between SLR residuals and solar geometry is also examined. User-domain performance is evaluated using BDS-3 static PPP at 24 stations during January 2025. Finally, MEO-only solutions are compared with solutions combining MEO and inclined geosynchronous orbit (IGSO) satellites using products from the Center for Orbit Determination in Europe (CODE).

The remainder of this paper is organized as follows. Section 2 describes the MGEX products, the four ACs, and the methods used to assess orbit consistency, clock quality, and static PPP performance. Section 3 presents the results and discussion, organized by orbit quality, clock quality, and PPP performance—including the MEO-only versus MEO + IGSO comparison. Section 4 summarizes the main conclusions, identifies the limitations of this study, and outlines directions for future work.

2. Data and Methods

2.1. IGS MGEX Orbit and Clock Products

BDS precise orbit and clock products released by four ACs within the IGS MGEX framework [16] are evaluated: CODE, the German Research Centre for Geosciences (GFZ), the Information and Analysis Center for Positioning, Navigation and Timing (IAC), and Wuhan University (WHU). Products from all four ACs are obtained from the IGS Data Center at Wuhan University at http://www.igs.gnsswhu.cn/ (accessed on 9 November 2026). The data center provides access to GNSS observations and precise products through its observation and product archives, respectively [17]. The products cover the period from 1 January to 31 December 2025.

Table 1 summarizes the constellation coverage, orbit and clock sampling intervals, and support for geostationary Earth orbit (GEO) satellites for each AC. Among the four products, GFZ0MGXRAP is a rapid product, whereas COD0MGXFIN, IAC0MGXFIN, and WUM0MGXFIN are final products. All orbit products are provided at 5 min intervals. Clock products are available at both 30 s and 5 min intervals for some ACs, but only the 30 s products are used in this study. As summarized in Table 1, the selected GFZ products include both BDS-2 and BDS-3 GEO satellites, whereas the selected WHU products include only BDS-2 GEO satellites; the selected CODE and IAC products do not include GEO satellites. GEO satellites are therefore excluded to maintain a consistent comparison across the four ACs, and the present assessment is restricted to MEO and IGSO satellites.

Table 1. Summary of the MGEX BDS precise orbit and clock products evaluated in this study.

Analysis Center	Product Name	Orbit Sampling Interval	Clock Sampling Interval	BDS-2	BDS-3
CODE	COD0MGXFIN	5 min	30 s/5 min	GEO not included	GEO not included
GFZ	GFZ0MGXRAP	5 min	30 s/5 min	Supported	Supported
IAC	IAC0MGXFIN	5 min	30 s	GEO not included	GEO not included
WHU	WUM0MGXFIN	5 min	30 s	Supported	GEO not included

The nominal MEO and IGSO orbital altitudes are approximately 21,528 and 35,786 km, respectively, with inclinations of approximately 55° [1,18]. These correspond to semi-major axes of approximately 27,906 and 42,164 km and Keplerian orbital periods of approximately 12.89 and 23.93 h, respectively. Both orbit types are near-circular. MEO satellites provide global coverage through their motion across multiple orbital planes, whereas IGSO satel-

lites have figure-eight ground tracks and provide prolonged visibility over their principal service region.

Table 2 lists the BDS satellites included in this study, along with orbit types, manufacturers, and pseudo-random noise (PRN)–SVN assignments in 2025 [19]. The complete BDS-3 MEO constellation comprises 14 satellites manufactured by the China Academy of Space Technology (CAST) and 10 by the Shanghai Engineering Center for Microsatellites (SECM). Since C222 (PRN C46) is not available in the selected products, our BDS-3 sample comprises 23 MEO satellites and 3 IGSO satellites.

Table 2. BDS satellites and their 2025 PRN–SVN assignments, orbit types, and manufacturers. C222 (PRN C46) is excluded from the analysis because it is unavailable in the selected products.

System	Orbit Type	Number of Satellites	SVN (PRN Valid in 2025)	Manufacturer
BDS-2	MEO	3	C012 (C11), C013 (C12), C015 (C14)	CAST
	IGSO	7	C005 (C06), C007 (C07), C008 (C08), C009 (C09), C010 (C10), C017 (C13), C019 (C16)	CAST
BDS-3	MEO	13	C201 (C19), C202 (C20), C205 (C22), C206 (C21), C209 (C23), C210 (C24), C213 (C32), C214 (C33), C218 (C36), C219 (C37), C223 (C45), C227 (C41), C228 (C42)	CAST
	MEO	10	C203 (C27), C204 (C28), C207 (C29), C208 (C30), C211 (C26), C212 (C25), C215 (C35), C216 (C34), C225 (C44), C226 (C43)	SECM
	IGSO	3	C220 (C38), C221 (C39), C224 (C40)	CAST

The precise orbit determination (POD) strategies adopted by the four ACs are compared in Table 3. All ACs process B1I and B3I signals. The IGS20 antenna model provides satellite and receiver antenna phase center offset (PCO) and phase center variation (PCV) corrections [20]. CODE uses double-difference processing, while GFZ, IAC, and WHU adopt undifferenced processing. The orbit arc lengths of the four ACs range from 24 h to 72 h, and their elevation cutoff angles from 3° to 10°.

Table 3. Precise orbit determination strategies adopted by the selected MGEX ACs. Processing strategies were compiled from the Analysis Strategy Summary (ACN) files released by the individual ACs and the summary provided by Steigenberger et al. [11]. The WHU entries were supplemented and cross-checked against Guo et al. [13]. PCO, phase center offset; PCV, phase center variation; SRP, solar radiation pressure; R, radial; A, along-track; C, cross-track; β, elevation angle of the Sun above the orbital plane.

Items	CODE	GFZ	IAC	WHU
Software	Bernese GNSS Software [21]	EPOS.P8 [22]	STARK [23]	PANDA [24]
Observation processing	Double-difference	Undifferenced	Undifferenced	Undifferenced
Signals	B1I/B3I	B1I/B3I	B1I/B3I	B1I/B3I
Orbit/clock sampling	5 min/30 s	5 min/30 s	5 min/30 s	5 min/30 s
Elevation cutoff angle	3°	3°	7°	10°
Orbit arc length	72 h	24 h	48 h	24 h
Ambiguity resolution	Fixed	Fixed	Fixed	Fixed

Table 3. *Cont.*

Items	CODE	GFZ	IAC	WHU
Inter-system bias (ISB)	24 h ISB	24 h ISB; separate ISBs for BDS-2 and BDS-3	48 h ISB	24 h ISB
Receiver antenna PCO/PCV	IGS20	IGS20	IGS20	IGS20
Satellite antenna PCO/PCV	IGS20	IGS20	IGS20	IGS20
CAST attitude model	Dilssner [25]	Wang et al. [26]	Dilssner [25]	Wang et al. [26]
SECM attitude model	Dilssner [25]	Zhao et al. [27]	Dilssner [25]	Lin et al. [28]
A priori BDS-3 SRP model	None	None	Box-wing model based on CSNO metadata [29]	Empirical SRP model for BDS-3 CAST and SECM satellites [30]
Solar radiation pressure model	ECOM-2: D0, Y0, B0, BC, BS, D2C, D2S	Reduced ECOM: D0, Y0, B0, BC, BS	ECOM-based: SC, Y0, BC, BS; D0 and B0 for $\lvert\beta\rvert \leq 5°$; D1C and D1S for $\lvert\beta\rvert > 5°$	Reduced ECOM: D0, Y0, B0, BC, BS
Antenna thrust	Applied	Applied	Applied	Applied
Earth albedo	Not applied	Not applied	Applied [31]	Applied [13]
Pseudo-stochastic pulses	Every 12 h in R/A/C	At noon in R/A/C	At noon in R/A/C	Not applied

For satellite attitude modeling, CODE and IAC apply the yaw attitude model of Dilssner [25] to both CAST and SECM satellites. GFZ applies the models of Wang et al. [26] and Zhao et al. [27] for CAST and SECM satellites, respectively, whereas WHU adopts the models of Wang et al. [26] and Lin et al. [28].

The SRP modeling strategies vary considerably among ACs. CODE applies the seven-parameter Empirical CODE Orbit Model 2 (ECOM-2) [32], whereas GFZ and WHU estimate the five-parameter reduced Empirical CODE Orbit Model (reduced ECOM) [33,34]. IAC adopts an ECOM-based parameterization that varies with β, the elevation angle of the Sun above the orbital plane [11]. CODE and GFZ do not apply an a priori BDS-3 SRP model. IAC uses a box-wing model based on metadata from the China Satellite Navigation Office (CSNO) [11,29]. WHU uses the empirical a priori SRP model developed by Wang [30] for BDS-3 CAST and SECM satellites [13]. Antenna thrust is modeled by all ACs, whereas Earth albedo is considered only by IAC and WHU. CODE estimates pseudo-stochastic pulses in the radial, along-track, and cross-track directions every 12 h; GFZ and IAC estimate corresponding pulses at orbital noon; WHU does not apply pseudo-stochastic pulses.

2.2. Orbit Quality Assessment

Orbit quality is assessed through inter-center orbit comparisons and SLR validation. Inter-center comparisons quantify the relative consistency of orbit products, whereas SLR provides external validation independent of GNSS microwave observations.

2.2.1. Orbit Consistency Analysis

Orbit consistency is evaluated through pairwise comparisons of satellite positions from the precise orbit products. At common epochs, satellite coordinates are transformed from the Earth-fixed frame to a common geocentric inertial frame using the corresponding Earth rotation parameters. Position differences are then resolved into radial (R), along-track (A), and cross-track (C) components using the first product in each AC pair as the reference orbit.

The reference-orbit velocity used to construct the RAC frame is obtained by analytically differentiating a seventh-degree polynomial interpolant of the satellite positions.

To reduce the influence of orbital maneuvers, product discontinuities, and anomalous epochs, median absolute deviation (MAD)-based screening is applied separately to each RAC component for every AC-pair–satellite combination. An observation is classified as an outlier when its deviation from the median exceeds three times the scaled MAD, using a scale factor of 1.4826 [35]. If any RAC component exceeds this threshold, the corresponding epoch is removed from all three RAC component series. After screening, the RMS values of the R, A, and C differences are calculated for each satellite. Group-level three-dimensional (3D) RMS values are recalculated from all valid RAC differences for the satellites and epochs within each group defined by BDS constellation and orbit type. These metrics represent the relative orbit consistency between two ACs rather than the absolute orbit accuracy of either product.

2.2.2. SLR Validation Method

SLR observations are independent of GNSS microwave observations. SLR can be used to assess force models in precise orbit determination [36,37] and is also widely used for external validation of precise orbits of low Earth orbit satellites [38] and GNSS satellites [39–42]. ILRS tracks only a subset of BDS satellites [43]. The 2025 dataset contains valid normal-point observations for four BDS-2 satellites and 21 BDS-3 MEO satellites. These observations were obtained from the EUROLAS Data Center (EDC) operated by Deutsches Geodätisches Forschungsinstitut of the Technical University of Munich.

For each normal point, the SLR residual is defined as the difference between the corrected SLR range and the geometric range computed from the precise orbit and station coordinates [44]. This validation uses the precise orbit products provided by the ACs as input, and the SLR observations are used only to compute residuals, without re-estimating the satellite orbits or fitting force model parameters to the SLR data. Table 4 lists the models and corrections applied in the residual computation. Station positions and velocities are taken from SLRF2020 [45]. The solution segment valid for each station is selected, and the coordinates are propagated using the supplied velocities to the midpoint of each daily session, with the applicable post-seismic deformation (PSD) correction applied. The annual and semiannual station coordinate corrections provided with ITRF2020 are not applied. The propagated coordinates are held fixed in the daily validation; tidal displacements are modeled at the observation epochs. An elevation cutoff of 3° is applied. Satellite-specific laser retroreflector array (LRA) offsets relative to the center of mass (CoM) are obtained from CSNO metadata [29], with numerical values available from the ILRS array-offset table [46]. Tropospheric delays are modeled using the Mendes–Pavlis model [47], and ocean tidal loading is modeled using FES2014b [48]. Solid Earth tides are corrected using TIDE2000 [49]. Pole tide, atmospheric tidal loading, and relativistic effects follow IERS Conventions 2010 [50].

For each AC and satellite, residuals with absolute values greater than 50 cm are first removed. The remaining residuals are screened using the MAD-based criterion described in Section 2.2.1. After quality control, the mean residual and standard deviation (STD) are calculated for each satellite and satellite group. The mean residual characterizes the systematic offset between the observed and modeled ranges, whereas the STD describes residual dispersion. Since SLR is primarily sensitive to radial orbit errors, radial orbit quality is assessed independently, whereas along-track, cross-track, and clock errors are not fully characterized [7].

Table 4. Models and parameters used for SLR validation.

Items	SLR Strategy
Software	Bernese GNSS Software 5.4
Precise products	Precise orbit and Earth rotation parameter products
Station reference frame	SLRF2020
Elevation cutoff	3°
Solid Earth tide	TIDE2000
Pole tide	IERS Conventions 2010
Ocean tidal loading	FES2014b
Atmospheric tidal loading	IERS Conventions 2010
Tropospheric delay model	Mendes–Pavlis model
Relativistic effects	IERS Conventions 2010
LRA offset	CSNO metadata [29]; numerical LRA–CoM offsets from ILRS [46]

2.3. Clock Quality Assessment

Clock products are evaluated in terms of inter-center consistency and apparent frequency stability. Clock-consistency analysis quantifies relative differences after clock-datum alignment, whereas ADEV characterizes apparent frequency stability over different integration times.

2.3.1. Clock Consistency Analysis

Since different ACs impose different datum constraints during satellite clock estimation, directly differencing two clock products introduces arbitrary datum offsets unrelated to the actual quality of the clocks. The datums are therefore aligned following Steigenberger and Montenbruck [5] in three steps: (i) calculating the raw clock difference at each common epoch, (ii) removing a daily satellite-specific offset, and (iii) removing an epoch-wise common offset across the BDS constellation. For ACs A and B:

$$d_s(t) = \delta t_s^A(t) - \delta t_s^B(t) \tag{1}$$

$$d'_s(t) = d_s(t) - \frac{1}{N_s} \sum_{t_j \in T_s} d_s\left(t_j\right) \tag{2}$$

$$e_s(t) = d'_s(t) - \frac{1}{M_t} \sum_{r \in S_t} d'_r(t) \tag{3}$$

where $\delta t_s^A(t)$ and $\delta t_s^B(t)$ are the clock offsets of satellite s at epoch t from ACs A and B. Equation (1) forms the raw difference $d_s(t)$ at the common epochs, which still contains two datum contaminants: a constant (daily) offset that differs per satellite, and a time-varying offset common to all satellites at a given epoch. Equations (2) and (3) remove these in turn. In Equation (2), T_s and N_s denote the set and number of common valid epochs for satellite s on the current day; subtracting the daily mean removes the satellite-specific offset and yields $d'_s(t)$. In Equation (3), S_t and M_t denote the set and number of satellites with valid clocks at epoch t; since the remaining datum error affects all satellites equally, subtracting the across-satellite mean at each epoch removes it, yielding the datum-aligned residual $e_s(t)$. The resulting datum-aligned residual $e_s(t)$ is used to assess relative clock consistency between the two products.

For each AC pair and satellite, anomalous epochs are removed from the clock-residual series using the MAD-based criterion described in Section 2.2.1. The retained residuals are converted to nanoseconds, and an RMS value is calculated separately for each satellite. Group-level RMS values are recalculated from all valid residuals for the satellites and epochs within each group defined by BDS constellation and orbit type. These RMS values quantify relative clock consistency between ACs rather than the absolute error of either product

with respect to an external time scale. Clock-residual RMS values are also expressed as centimeter-equivalent one-way range differences using $\Delta\rho = c\Delta t$, where c is the speed of light. A clock difference of 0.1 ns corresponds to approximately 3.0 cm in equivalent range.

2.3.2. Allan Deviation Analysis

ADEV is a widely used time-domain measure of the fractional-frequency stability of atomic clocks [51]. Short integration times mainly characterize rapid clock fluctuations, whereas longer integration times are more sensitive to drift, periodic variations, and low-frequency errors [52]. Daily ADEV values are calculated independently for each satellite using the original clock-offset series provided by each AC. For an integration time τ, ADEV is defined as

$$\sigma_y(\tau) = \sqrt{\frac{1}{2(N-2)\tau^2}\sum_{i=1}^{N-2}(x_{i+2} - 2x_{i+1} + x_i)^2} \quad (4)$$

where x_i is a clock-offset sample at interval τ, and N is the number of valid samples. ADEV is dimensionless, and a lower value at a given τ indicates better apparent frequency stability [9].

For each AC and satellite, daily ADEV values at each integration time are summarized by the annual median. The annual median curve characterizes the time-scale-dependent stability of each clock product. For comparisons among ACs, BDS systems, and orbit types, group-level ADEV values at $\tau = 9000$ s are calculated as the median of all valid daily satellite ADEV estimates within each group. This particular integration time is representative of medium-term clock behavior and is known to capture systematic variations that may arise from orbit-modeling errors [11]. Since radial orbit errors can be mapped into estimated satellite clock offsets, the resulting ADEV represents the apparent stability of the clock products rather than the intrinsic physical stability of the onboard atomic clocks.

2.4. Static PPP Processing

Precise orbit and clock products are used in PPP to provide high-accuracy positioning from a single GNSS receiver and thereby evaluate their combined performance in the user domain [53]. A BDS-3 static PPP analysis is conducted from 1 to 31 January 2025 using daily Receiver Independent Exchange Format (RINEX) observation files downloaded from the IGS Data Center at Wuhan University.

Figure 1 shows the global distribution of the 24 IGS/MGEX tracking stations. The stations are grouped into the Americas, Europe–Africa, Asia–Pacific, and Antarctica (Table 5). In the primary comparison among the four products, each PPP solution incorporates all BDS-3 MEO and IGSO satellites available in the corresponding product.

Table 5. Regional grouping of IGS/MGEX tracking stations employed for PPP evaluation.

Region	Number of Stations	Stations
Americas	6	HOLB, YEL2, STJ3, BOGT, CUIB, RGDG
Europe–Africa	7	YEBE, MAR6, ORID, YKRO, MBAR, SUTH, ABPO
Asia–Pacific	7	URUM, IISC, NTUS, WUH2, DARW, MRO1, ALIC
Antarctica	4	OHI3, MAW1, DAV1, CAS1

Station coordinates from the corresponding IGS weekly combined solutions in Solution Independent Exchange Format (SINEX), aligned to the IGS20 reference frame, are used as reference values. These weekly solutions are formed by combining station-coordinate estimates submitted by the contributing IGS ACs. For each station-day, the difference be-

tween the PPP coordinate estimate and the corresponding weekly IGS reference coordinate is computed in the Earth-fixed frame. The resulting coordinate differences are then transformed into local east (E), north (N), and up (U) components. Component RMS values are calculated from the daily ENU coordinate differences relative to these reference coordinates. The 3D RMS is the root-sum-square of the three component RMS values. Regional and overall RMS values are calculated from all valid station-day coordinate differences within each subset.

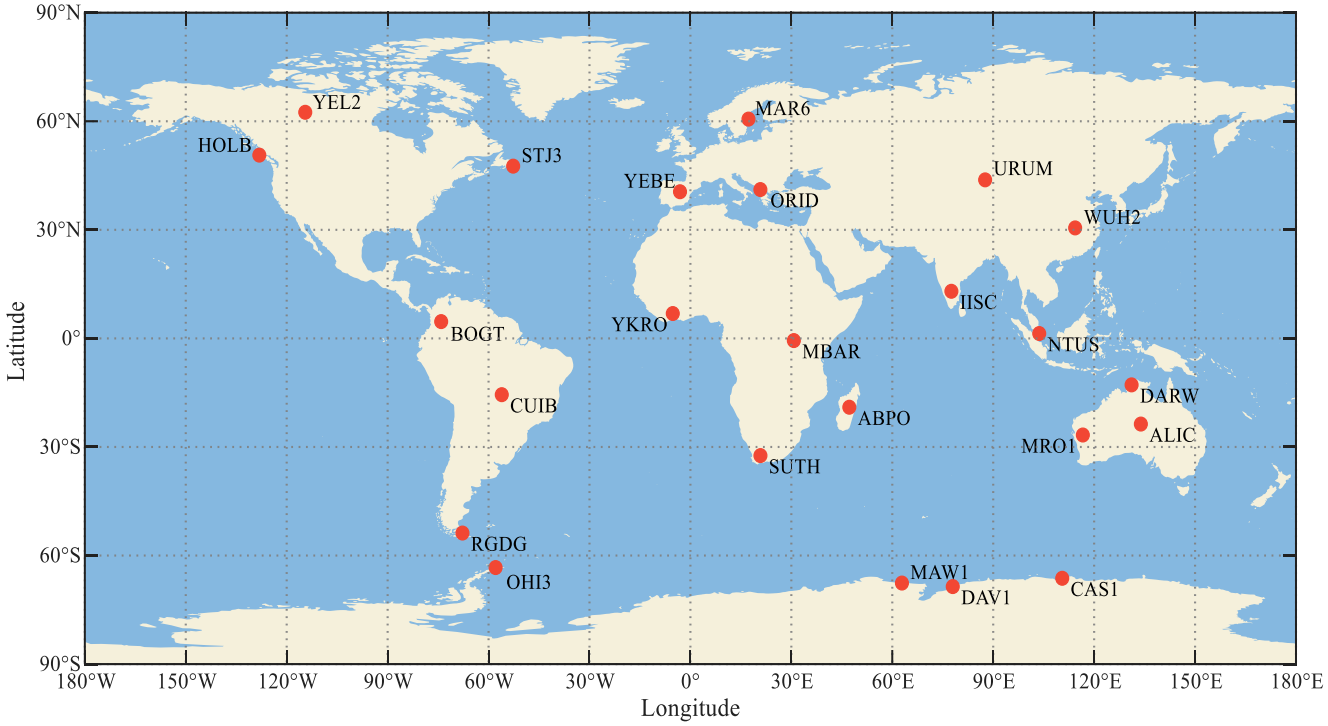


Figure 1. Global distribution of the 24 IGS/MGEX stations used for BDS-3 static PPP.

Table 6 summarizes the principal PPP processing settings. All solutions are generated with Bernese GNSS Software using undifferenced BDS-3 observations and least-squares estimation. Data are processed at 30 s intervals with a 10° elevation cutoff. Elevation-dependent weighting is applied as $w(e) = sin^2(e)/{\sigma_0}^2$, where e is the satellite elevation angle and σ_0 is the zenith standard deviation of the corresponding code or phase observable. Carrier-phase wind-up is corrected using the modeled satellite attitude and receiver antenna orientation [54]. Relativistic corrections include the periodic eccentricity-related satellite-clock term and Shapiro delay [55]. Earth rotation during signal propagation (the Sagnac effect) is accounted for in the range model [55]. Station coordinates are estimated as daily constants, and receiver clock offsets are estimated independently at each epoch. Zenith wet delays are estimated as station-specific parameters, whereas carrier-phase ambiguities are estimated as float parameters.

Table 6. Processing strategy for BDS-3 static PPP in January 2025.

Items	PPP Strategies
Software	Bernese GNSS Software 5.4
Precise products	Precise orbit, clock, and Earth rotation parameter products from the corresponding AC
Satellite system	BDS-3 MEO and IGSO

Table 6. *Cont.*

Items	PPP Strategies
Observation type	Pseudorange and carrier-phase observations
Observation signals	B1I/B3I ionosphere-free linear combination
Sampling interval	30 s
Elevation cutoff angle	10°
Observation weighting	$w(e) = sin^2(e)/{\sigma_0}^2$
A priori standard deviations of code and phase	0.1 m/0.001 m
Antenna PCO/PCV correction	IGS20
Ionospheric delay	First-order ionospheric delay eliminated by the ionosphere-free combination
Tropospheric delay and mapping function	Zenith hydrostatic delay modeled with GPT3; zenith wet delay estimated as a parameter; hydrostatic and wet mapping coefficients obtained from GPT3 [56]
Ocean tide loading	FES2014b [48]
Tidal corrections	Solid Earth tide and pole tide corrected according to IERS Conventions 2010 [50]
Phase wind-up	Corrected [54]
Relativistic effect	Corrected [55]
Sagnac effect	Corrected [55]
Estimation method	Least-squares estimation
Receiver clock offset	Estimated epoch-wise
Zenith wet delay	Estimated as a station-specific tropospheric parameter
Phase ambiguity	Estimated as float parameters
Station coordinates	Estimated as constant parameters in each daily solution

3. Results and Discussion

3.1. Orbit Quality Assessment Results

3.1.1. Orbit Consistency

Figure 2 presents the annual RMS values of the orbit differences in R, A, and C directions for individual satellites and each AC pair. Most BDS-3 MEO satellites show component RMS values of approximately 2–5 cm, while larger differences are confined to a few satellites. C005 shows a predominantly along-track discrepancy exceeding 20 cm in pairs involving CODE. By contrast, the BDS-3 IGSO satellites C220, C221, and C224 show larger radial RMS differences of 13.31–21.93 cm in pairs involving WHU. The BDS-3 MEO satellites C211, C212, C215, and C223 also exhibit increased radial RMS differences in pairs involving WHU, ranging from 3.47 to 12.88 cm.

Table 7 summarizes the annual 3D RMS orbit differences for BDS-2 and BDS-3 satellites by orbit type and AC pair. For the same AC pairs, the BDS-3 MEO 3D RMS values are 38.3–59.9% lower than those of BDS-2 MEO. This higher consistency agrees with earlier findings, which identified increased tracking coverage, the fully populated MEO constellation, and improved SRP modeling as possible contributors [11]. The largest group-level differences occur for BDS-3 IGSO satellites in pairs involving WHU, with 3D RMS values of 17.86–19.99 cm. For WHU specifically, the improved a priori SRP model described by Guo et al. [13] has been applied to BDS-3 MEO products, but the corresponding optimization

has not been implemented for BDS-3 IGSO products. This difference, together with differences in attitude modeling and other processing strategies, may contribute to the larger discrepancies involving WHU. Across both BDS-2 and BDS-3, MEO products have higher inter-center consistency than IGSO products. The lower consistency of IGSO products may partly reflect regional tracking coverage and difficulties in radiation-pressure modeling associated with their elongated bodies and additional communication antennas [3,11]. Both orbit-type characteristics and AC-dependent processing may contribute to these differences, although inter-center comparisons alone cannot isolate their contributions.

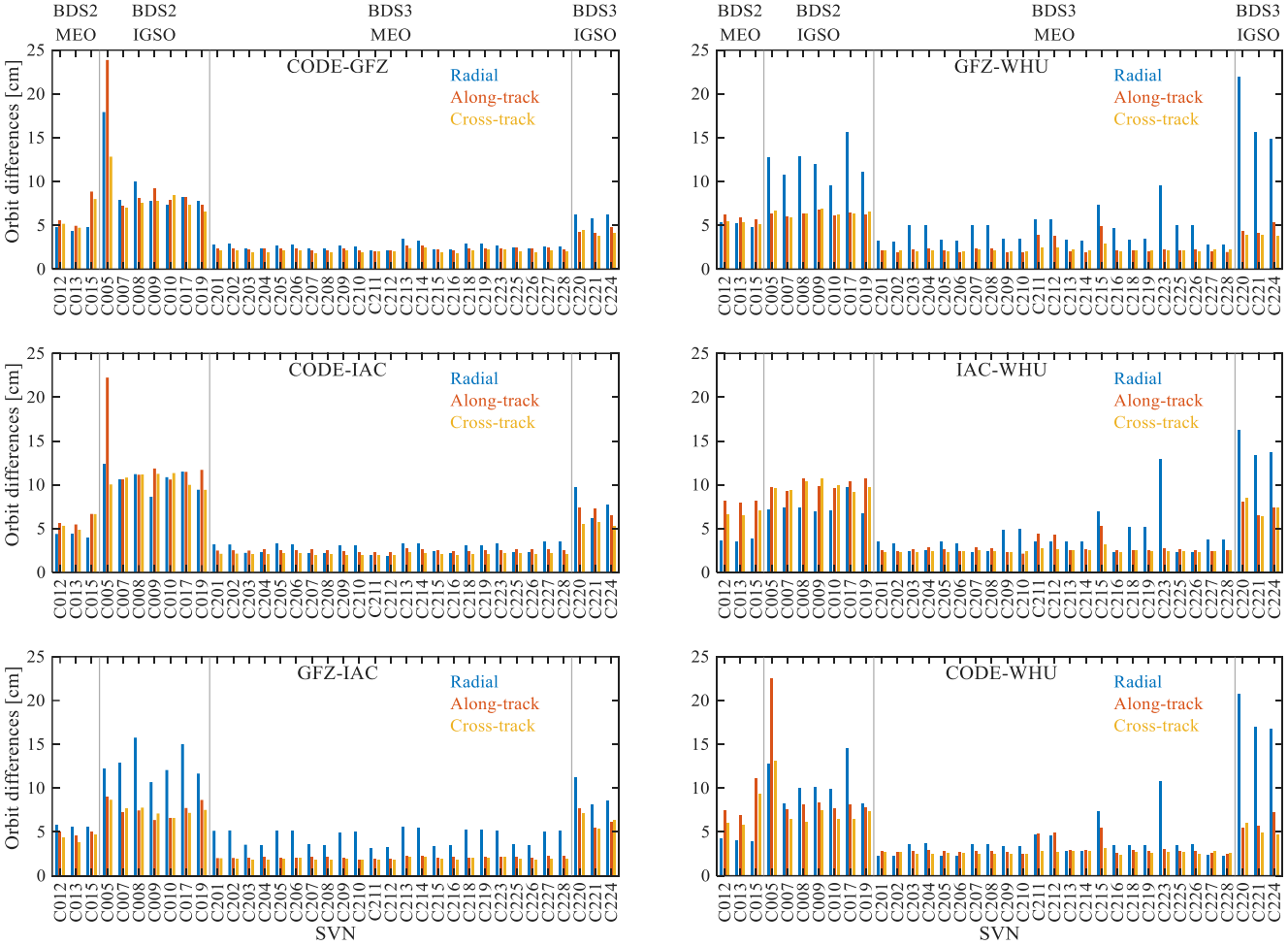


Figure 2. Satellite-wise annual RMS values of R, A, and C orbit differences for each AC pair in 2025. Vertical grey lines separate satellite groups by constellation and orbit type.

Table 7. Summary of annual 3D RMS orbit differences for BDS-2 and BDS-3 satellites by orbit type (MEO and IGSO) across all AC pairs.

AC1	AC2	BDS-2		BDS-3	
		MEO [cm]	IGSO [cm]	MEO [cm]	IGSO [cm]
CODE	GFZ	10.23	17.94	4.10	8.59
CODE	IAC	9.24	20.14	4.29	12.01
CODE	WHU	12.19	17.53	5.86	19.99
GFZ	IAC	8.66	16.86	5.34	13.08
GFZ	WHU	9.48	15.26	5.74	18.80
IAC	WHU	11.13	15.95	5.92	17.86

3.1.2. SLR Validation

Figure 3 presents the annual means and STDs of satellite-wise SLR residuals, and Table 8 summarizes the grouped statistics. Most BDS-3 MEO satellites show STDs of approximately 2–4 cm, while several satellites exhibit larger dispersion. A similar satellite-dependent pattern was reported by Zajdel et al. [14], with STDs of approximately 1.9–2 cm for 14 BDS-3 MEO satellites and substantially larger values for several others.

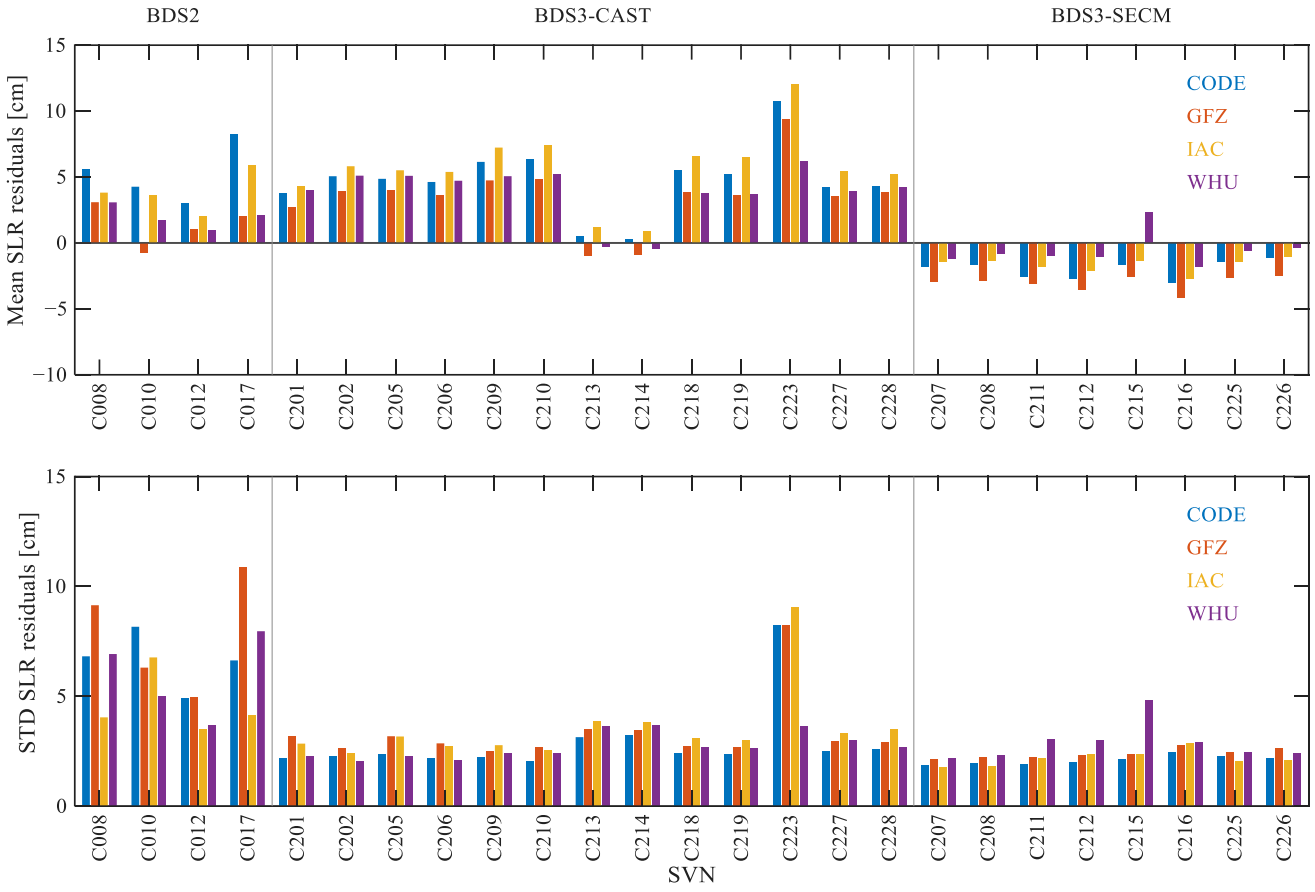


Figure 3. Satellite-wise annual means and STDs of SLR residuals for the four MGEX products in 2025. Vertical grey lines separate the BDS-2, BDS-3 CAST, and BDS-3 SECM groups.

Table 8. Annual SLR residual statistics for BDS-2, BDS-3 CAST, and BDS-3 SECM satellites.

AC	BDS-2		BDS-3 CAST		BDS-3 SECM	
	Mean [cm]	STD [cm]	Mean [cm]	STD [cm]	Mean [cm]	STD [cm]
CODE	5.13	6.81	4.73	3.90	−1.93	2.15
GFZ	1.41	8.14	3.58	4.17	−3.00	2.42
IAC	3.63	4.79	5.61	4.45	−1.59	2.18
WHU	1.87	6.09	4.03	3.22	−0.64	3.01

At the group level, BDS-2 shows positive mean residuals of 1.41–5.13 cm and STDs of 4.79–8.14 cm across the four products. Including C223, the BDS-3 CAST group shows positive means of 3.58–5.61 cm, whereas the SECM group shows negative means of −3.00 to −0.64 cm. Their grouped STDs are 3.22–4.45 cm and 2.15–3.01 cm, respectively, both lower than those of BDS-2.

The opposite signs of the CAST and SECM mean residuals are consistent with previous findings [13,44]. Such manufacturer-dependent offsets may partly reflect differences in

spacecraft geometry, particularly the different elongation directions of the satellite bodies, and limitations in radiation-pressure modeling [44]. However, these offsets cannot be uniquely attributed to radiation-pressure modeling, because uncertainties in satellite antenna phase center offsets, LRA–CoM offsets, and station-dependent range biases may also contribute [14].

Figure 4 relates the residuals of C211, C212, C215, and C223 to the solar elongation angle ε, defined as the angle between the Earth and Sun directions at the satellite. Colors indicate β, the elevation angle of the Sun above the orbital plane. C211 and C212 show modest negative slopes across the four products. C215 exhibits an increasing trend with ε for WHU but decreasing trends for CODE, GFZ, and IAC. C223 shows stronger ε-related variations in the CODE, GFZ, and IAC solutions, with large positive residuals occurring mainly at large negative β, whereas WHU shows weaker variations. The contrasting SLR residual patterns for C215 and C223 in the WHU and other AC products are consistent with the larger radial orbit differences involving WHU shown in Figure 2.

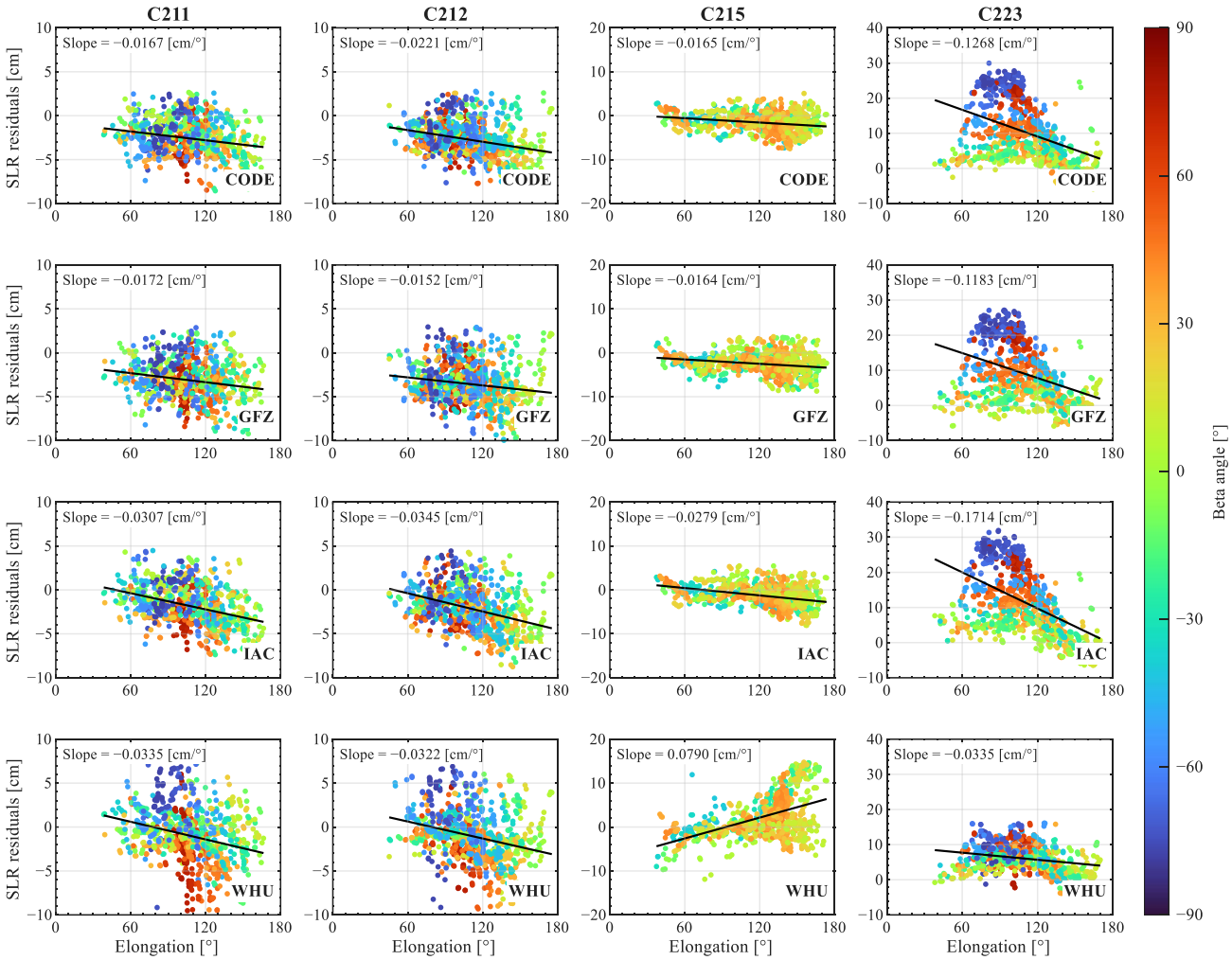


Figure 4. SLR residuals versus the solar elongation angle ε for selected BDS-3 satellites (C211, C212, C215, and C223) using CODE, GFZ, IAC, and WHU orbit products in 2025. Colors indicate β, the elevation angle of the Sun above the orbital plane; black lines show linear fits. Vertical scales are shared among ACs within each satellite column but differ between columns.

These solar-geometry-dependent patterns suggest possible limitations in SRP and attitude modeling. Guo et al. [13] showed that improved a priori SRP modeling reduced solar-elongation-dependent residual errors. Attitude model inaccuracies may also affect

radiation force modeling and observation corrections, especially during low-β yaw maneuvers [57]. For C223, Xie et al. [15] identified anomalies at large |β| and suggested that its search-and-rescue payload configuration and self-shadowing may contribute to the observed behavior. Taken together, the orbit comparisons and SLR validation provide complementary perspectives on these product differences. Improving SRP and attitude modeling may help reduce these solar-geometry-dependent residual variations, particularly for C215 in the WHU solution and C223 in the CODE, GFZ, and IAC solutions.

3.2. Clock Quality Assessment Results

3.2.1. Clock Consistency

Figure 5 presents the clock-residual RMS values for each individual satellite and AC pair. Most BDS-3 MEO values are below 0.15 ns (4.5 cm in equivalent range), whereas IGSO satellites show wider inter-center differences. C005 reaches approximately 0.4–0.6 ns (12.0–18.0 cm in equivalent range) in several pairs involving CODE. C215, C220, C221, and C224 show notably larger values in pairs involving WHU. The grouped statistics confirm that MEO clock products are more consistent than IGSO products for every AC pair (Table 9). BDS-3 MEO RMS values are 15.8–50.0% lower than those of BDS-2 MEO, while the RMS values for BDS-3 IGSO pairs involving WHU reach 0.40–0.52 ns (12.0–15.6 cm in equivalent range). Overall, BDS-3 MEO clock products are more consistent across ACs, whereas IGSO clock products show larger differences, particularly for some AC pairs.

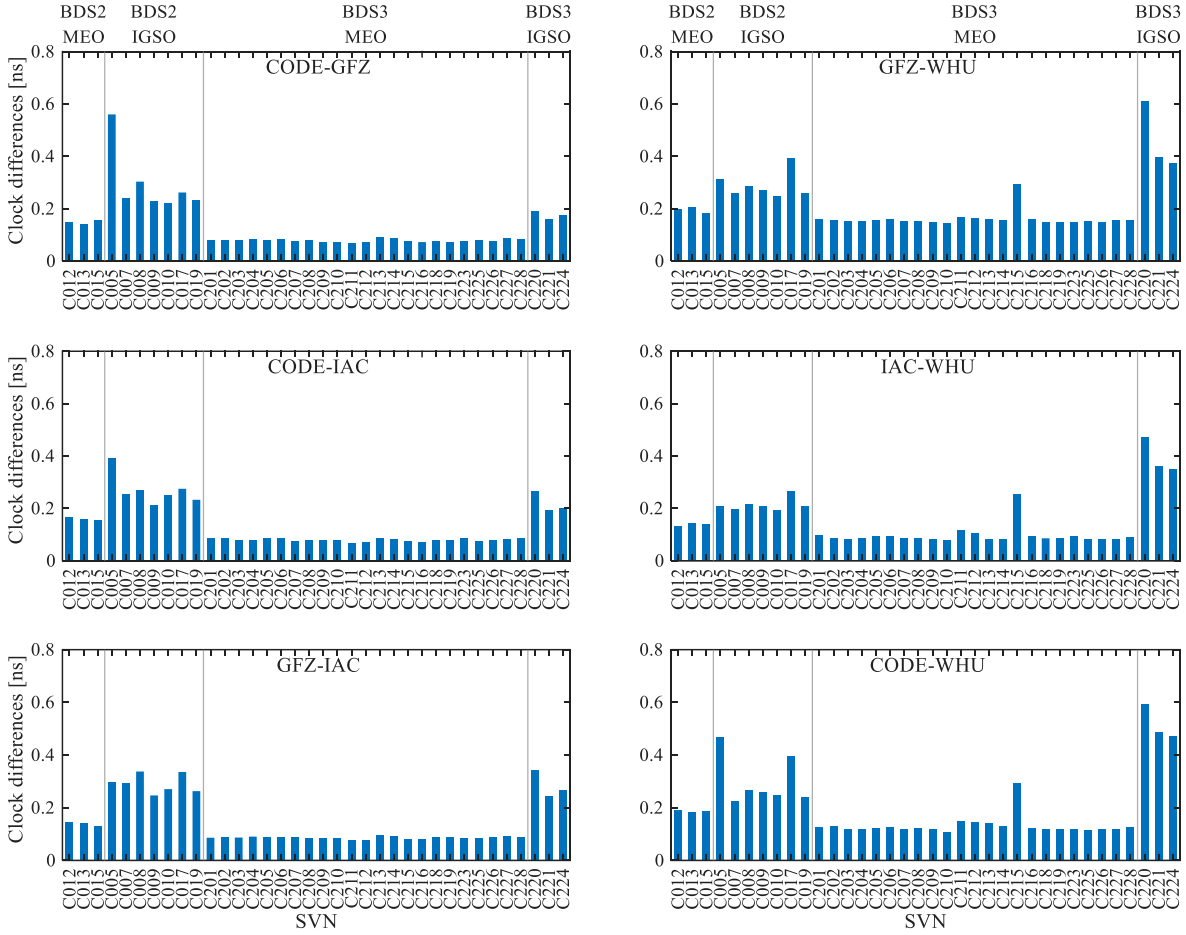


Figure 5. Satellite-wise annual clock-residual RMS values for each AC pair in 2025. Each 0.2 ns tick interval corresponds to approximately 6.0 cm in equivalent range. Vertical grey lines separate satellite groups by constellation and orbit type.

Table 9. Annual clock-residual RMS values for BDS-2 and BDS-3 MEO and IGSO satellites. Values are given in nanoseconds, with centimeter-equivalent range differences in parentheses.

AC1	AC2	BDS-2		BDS-3	
		MEO [ns (cm)]	IGSO [ns (cm)]	MEO [ns (cm)]	IGSO [ns (cm)]
CODE	GFZ	0.15 (4.5)	0.32 (9.6)	0.08 (2.4)	0.18 (5.4)
CODE	IAC	0.16 (4.8)	0.28 (8.4)	0.08 (2.4)	0.22 (6.6)
CODE	WHU	0.19 (5.7)	0.31 (9.3)	0.14 (4.2)	0.52 (15.6)
GFZ	IAC	0.14 (4.2)	0.29 (8.7)	0.09 (2.7)	0.29 (8.7)
GFZ	WHU	0.19 (5.7)	0.29 (8.7)	0.16 (4.8)	0.47 (14.1)
IAC	WHU	0.14 (4.2)	0.21 (6.3)	0.10 (3.0)	0.40 (12.0)

Large clock-residual RMS values frequently coincide with large radial orbit differences for the same satellites and AC pairs. This correspondence is particularly evident for the WHU-related BDS-3 IGSO pairs and C215. It may partly reflect coupling between orbit and satellite-clock estimates during POD, since radial orbit errors can be absorbed by satellite-clock estimates [11]. For IGSO satellites, regional tracking coverage and radiation-pressure modeling pose additional challenges to orbit determination [11]. Differences in the ACs' orbit modeling and estimation strategies may therefore contribute to the wider inter-center clock differences.

3.2.2. Allan Deviation

Figure 6 presents the annual median ADEV curves for six selected BDS-3 satellites, comprising three MEO and three IGSO satellites, together with the corresponding 25th–75th percentile intervals. The WHU product shows noticeably wider percentile intervals at some integration times, indicating greater variability among the daily ADEV estimates. This may indicate that a noisy time datum has been chosen by WHU.

As shown in Figure 6, WHU shows larger ADEV values for C215, C220, C221, and C224 at medium and long integration times. Figure 7 compares the annual median ADEV values at $\tau = 9000$ s for individual BDS-2 and BDS-3 satellites across the four AC products. These four satellites also show larger values in the WHU product at this integration time. The larger ADEV values for C215 and the three BDS-3 IGSO satellites in the WHU product coincide with larger radial orbit differences involving WHU (Figure 2), consistent with possible orbit–clock coupling. For C215, WHU also shows a distinct solar-angle-dependent SLR residual trend (Figure 4). By contrast, the ADEV curves for C211 and C223 are similar across the four products (Figure 6). For C223, WHU also shows weaker solar-angle-dependent SLR variations than the other products (Figure 4). This may reflect a better fit of the WHU SRP model to the specific spacecraft configuration of C223. Through orbit–clock coupling, smaller solar-geometry-dependent orbit errors could also help explain why WHU does not show increased ADEV values for this satellite.

At the group level, Table 10 summarizes the median ADEV values at $\tau = 9000$ s. The BDS-2 IGSO values range from 6.71×10^{-14} to 7.24×10^{-14} across the four products. For BDS-3 IGSO satellites, the WHU value is 3.60×10^{-14}, compared with 1.72×10^{-14}, 1.69×10^{-14}, and 2.13×10^{-14} for CODE, GFZ, and IAC, respectively. To interpret these differences, the onboard clock types should also be considered. The BDS-3 MEO sample includes satellites equipped with rubidium clocks or passive hydrogen masers (PHMs), whereas the three BDS-3 IGSO satellites are equipped with PHMs [9,10]. However, clock type alone cannot explain differences among AC products for the same satellite, because these products refer to the same onboard clocks.

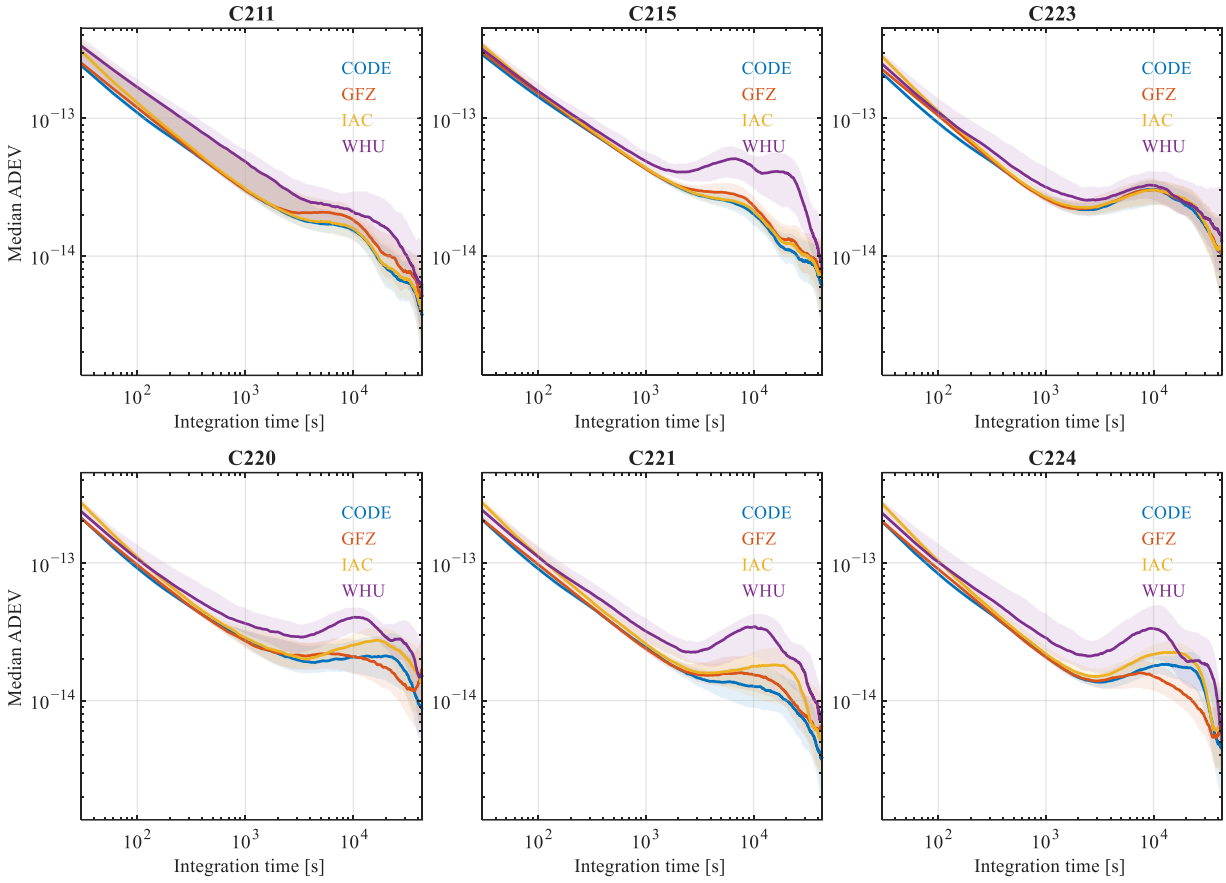


Figure 6. Annual median ADEV versus integration time for six selected BDS-3 satellites (C211, C215, C223, C220, C221, and C224) based on 2025 clock products from CODE, GFZ, IAC, and WHU. Shaded areas indicate the 25th–75th percentile ranges of daily ADEV values.

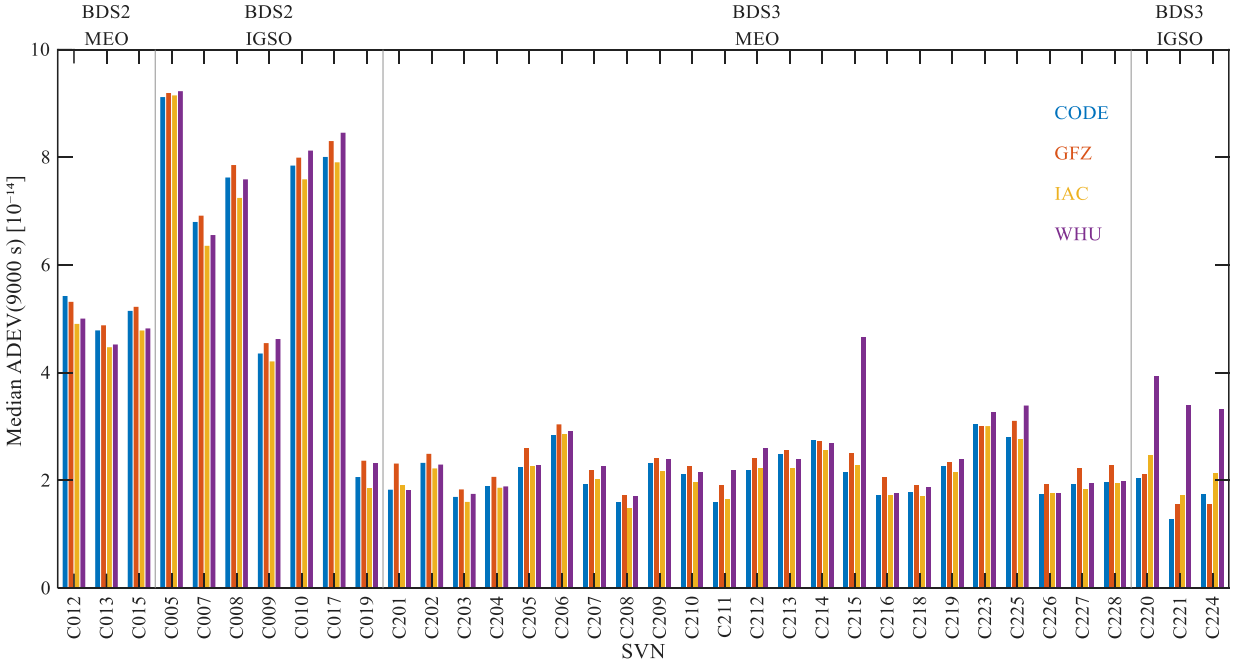


Figure 7. Satellite-wise annual median ADEV at an integration time of 9000 s for CODE, GFZ, IAC, and WHU in 2025. Vertical grey lines separate satellite groups by constellation and orbit type.

Table 10. Group-level median ADEV at $\tau = 9000$ s for BDS-2 and BDS-3 MEO and IGSO clock products from the four MGEX ACs. Values represent the median of all valid daily satellite ADEV estimates within each group.

AC	BDS-2		BDS-3	
	MEO	IGSO	MEO	IGSO
CODE	5.13×10^{-14}	6.95×10^{-14}	2.07×10^{-14}	1.72×10^{-14}
GFZ	5.13×10^{-14}	7.19×10^{-14}	2.32×10^{-14}	1.69×10^{-14}
IAC	4.70×10^{-14}	6.71×10^{-14}	2.03×10^{-14}	2.13×10^{-14}
WHU	4.77×10^{-14}	7.24×10^{-14}	2.24×10^{-14}	3.60×10^{-14}

Taken together, these results show lower inter-center consistency for both the WHU BDS-3 IGSO orbit and clock products, together with poorer apparent clock stability (Figures 2, 5 and 7; Tables 7, 9 and 10). Differences in SRP modeling and other processing strategies may contribute to the orbit discrepancies and affect clock estimates through orbit–clock coupling. Steigenberger et al. [11] reported similar increases for C220 and C224 near 10,000 s and suggested a relationship with β variations and orbit-modeling errors. Further investigation of the WHU BDS-3 IGSO products should therefore consider SRP modeling, attitude modeling, and possible noise in the clock datum.

3.3. BDS-3 Static PPP

3.3.1. Inter-Center Comparison

Figure 8 presents the RMS values of daily BDS-3 static PPP coordinate differences relative to the IGS weekly reference coordinates at the 24 stations. For all four products, the U component is generally larger than the E and N components. CODE exhibits the smallest errors across all three components, whereas WHU shows larger N and U errors at many stations. GFZ also shows comparatively large E-component errors at several stations, which may partly be associated with the use of rapid products. The grouped results confirm that CODE has the smallest overall PPP error, while the 3D RMS for WHU is approximately 2.6 times that for CODE (Table 11).

Table 11. Overall ENU and 3D RMS values of BDS-3 static PPP coordinate differences relative to the IGS weekly reference coordinates, January 2025.

AC	East [cm]	North [cm]	Up [cm]	3D [cm]
CODE	0.53	0.52	1.66	1.82
GFZ	1.94	0.84	2.23	3.07
IAC	0.85	0.79	2.57	2.82
WHU	1.33	1.94	4.09	4.72

Table 12 summarizes the station-averaged 1σ repeatability of daily coordinate solutions, calculated from the scatter about each station's mean position. CODE and IAC provide comparatively better repeatability than the other ACs. WHU yields marginally better repeatability than GFZ, although its 3D coordinate-difference RMS relative to the IGS reference coordinates is larger (Table 11). This contrast suggests that WHU products may include a relatively stable offset during January 2025. The larger WHU PPP errors coincide with anomalies in its BDS-3 IGSO and several MEO and clock products.

Table 12. Station-averaged 1σ repeatability of daily BDS-3 static PPP coordinate solutions using different MGEX products, January 2025.

AC	East [cm]	North [cm]	Up [cm]	3D [cm]
CODE	0.32	0.21	0.66	0.77
GFZ	1.74	0.52	1.27	2.24
IAC	0.51	0.34	0.97	1.16
WHU	0.91	0.72	1.67	2.07

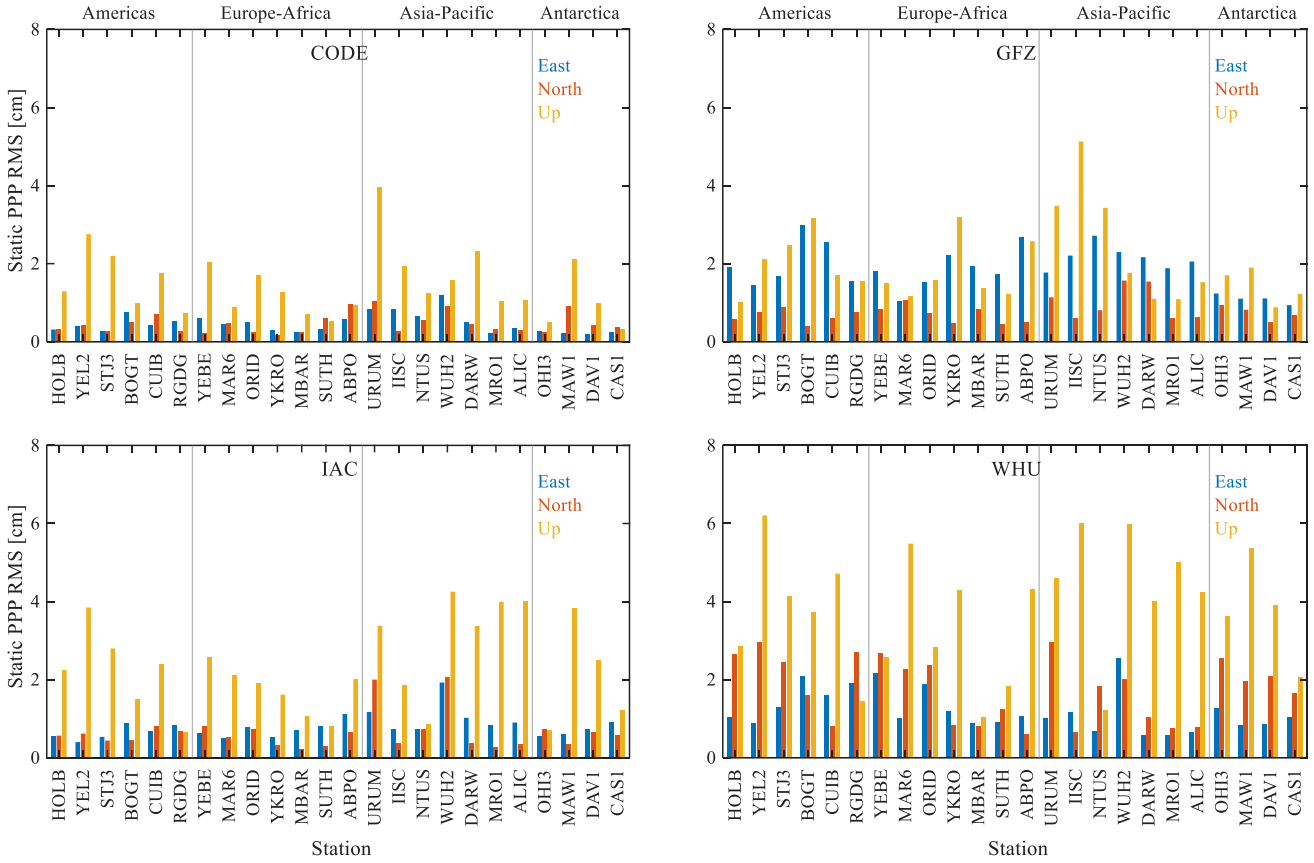


Figure 8. Station-wise RMS values of daily BDS-3 static PPP coordinate differences relative to the IGS weekly reference coordinates, January 2025. Vertical grey lines separate station groups by geographic region.

3.3.2. Impact of IGSO Satellites

To assess the impact of IGSO satellites on BDS-3 positioning, MEO-only and MEO + IGSO solutions are generated using CODE products under identical processing settings, including a 10° elevation cutoff. Both schemes are evaluated using the same 732 valid station-days at 24 stations. Figure 9 compares geometrically visible satellite counts and position dilution of precision (PDOP), calculated from CODE orbit positions at 5 min intervals. Table 13 summarizes the regional RMS values of coordinate differences relative to the IGS weekly reference coordinates. In the MEO-only solution, the four Antarctic stations, located between 63° S and 69° S, have the highest mean satellite visibility, the lowest PDOP, and the smallest 3D RMS of coordinate differences. In contrast, the seven Asia–Pacific stations, spanning 26.7° S–43.8° N, have the lowest mean satellite visibility, the highest PDOP, and the largest 3D RMS of coordinate differences.

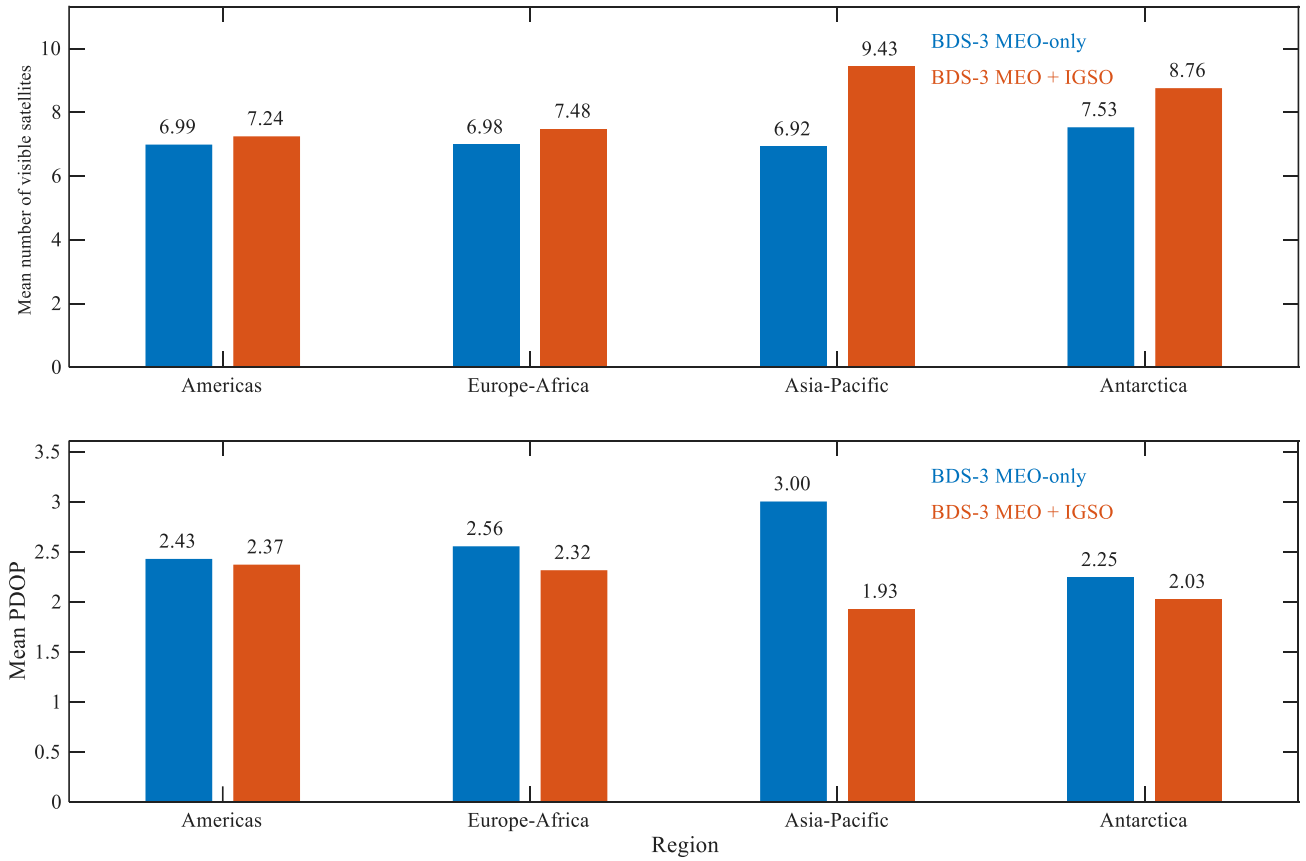


Figure 9. Regional mean geometrically visible satellite counts and PDOP for the CODE BDS-3 MEO-only and MEO + IGSO configurations in January 2025.

Table 13. Regional ENU and 3D RMS values of coordinate differences relative to the IGS weekly reference coordinates for CODE BDS-3 MEO-only and MEO + IGSO static PPP, January 2025.

Region	BDS-3 MEO-Only				BDS-3 MEO + IGSO			
	East [cm]	North [cm]	Up [cm]	3D [cm]	East [cm]	North [cm]	Up [cm]	3D [cm]
Americas	0.47	0.44	1.76	1.87	0.47	0.44	1.76	1.88
Europe–Africa	0.42	0.46	1.26	1.40	0.44	0.49	1.26	1.42
Asia–Pacific	0.81	0.69	2.03	2.29	0.73	0.61	2.11	2.31
Antarctica	0.34	0.56	1.00	1.20	0.24	0.53	1.16	1.30

Adding IGSO satellites increases satellite visibility and reduces PDOP in all regions, with the largest geometric improvement occurring in Asia–Pacific. In this region, the mean number of visible satellites increases from 6.92 to 9.43, while PDOP decreases by 35.7%, from 3.00 to 1.93. However, the regional 3D RMS values of coordinate differences remain similar or increase slightly (Table 13). This may be attributed to the larger errors in IGSO orbit and clock products compared with their MEO counterparts. Unless these accuracy differences are accounted for by appropriately down-weighting IGSO observations, the additional errors can offset the benefits of improved geometry. Developing an IGSO-specific weighting strategy is therefore a direction for future work.

4. Conclusions

The 2025 MGEX BDS precise orbit and clock products from CODE, GFZ, IAC, and WHU are assessed using inter-center comparisons, SLR validation, ADEV analysis, and BDS-3 static PPP. The main conclusions are as follows.

(1) Product consistency varies substantially among BDS orbit types. BDS-3 MEO products show the highest inter-center agreement, with 3D orbit-difference and clock-residual RMS values of 4.10–5.92 cm and 0.08–0.16 ns (2.4–4.8 cm in equivalent range), respectively. These values are 38.3–59.9% and 15.8–50.0% lower than those for BDS-2 MEO satellites. Larger differences occur for IGSO products, particularly in pairs involving WHU. For BDS-3 IGSO satellites, the corresponding orbit and clock RMS values reach 17.86–19.99 cm and 0.40–0.52 ns (12.0–15.6 cm in equivalent range), respectively. At $\tau = 9000$ s, the annual median ADEV of the WHU BDS-3 IGSO group is 3.60×10^{-14}, higher than those of the other three ACs. Taken together, these results suggest that the WHU BDS-3 IGSO products may benefit from a further assessment of the underlying attitude and SRP modeling.

(2) SLR residuals show manufacturer-specific and solar-geometry-dependent patterns. The CAST group shows positive mean residuals of 3.58–5.61 cm, whereas the SECM group shows negative means of −3.00 to −0.64 cm. Their STDs are 3.22–4.45 cm and 2.15–3.01 cm, respectively, both lower than the BDS-2 range of 4.79–8.14 cm. C215 shows a distinct trend in the WHU solution, while C223 shows stronger variations in the CODE, GFZ, and IAC solutions than in the WHU solution. These patterns identify satellites that warrant further investigation of satellite attitude and SRP modeling, as well as possible errors in satellite antenna phase center offsets and LRA–CoM offsets.

(3) Static PPP performance differs by several centimeters across the four AC products. The 3D RMS values of coordinate differences relative to the IGS weekly reference coordinates are 1.82, 3.07, 2.82, and 4.72 cm for CODE, GFZ, IAC, and WHU, respectively. The corresponding station-averaged 3D repeatabilities are 0.77, 2.24, 1.16, and 2.07 cm. Adding IGSO satellites increases visibility and reduces PDOP in all regions but does not improve coordinate accuracy. This indicates that improved observation geometry alone does not guarantee better PPP accuracy; residual errors associated with the added satellites may offset the geometric benefit.

Overall, the 2025 BDS-3 MEO products show high inter-center consistency, whereas IGSO satellites and two MEO satellites (C215 and C223) with pronounced solar-geometry-dependent SLR residual variations remain priorities for improving product reliability. These findings can support product selection, anomaly screening, weighting design, and quality control for future combined BDS products.

Several limitations should be acknowledged. Inter-center comparisons assess relative product consistency, whereas SLR primarily evaluates radial orbit quality. The PPP assessment is limited to 24 stations and one month of static data, and the MEO-only versus MEO + IGSO comparison uses only CODE products.

Author Contributions: Conceptualization and methodology, J.Q.; software, validation, formal analysis, investigation, data curation, and visualization, S.L.; writing—original draft preparation, S.L.; writing—review and editing, J.Q. and H.G.; supervision, H.G.; project administration, H.G.; funding acquisition, J.Q. and H.G. All authors have read and agreed to the published version of the manuscript.

Funding: This research was funded by the National Natural Science Foundation of China, grant number 42404028; the Shanghai Key Laboratory of Space Navigation and Positioning Techniques, grant number 202510; the Science and Technology Commission of Shanghai Municipality, grant number 24YF2747600; the Fundamental Research Funds for the Central Universities, grant number 22120260114; and the Joint Research Project of the Yangtze River Delta Science and Technology Innovation Community, grant number 2025CSJZN01900.

Data Availability Statement: The precise orbit, clock, and Earth rotation parameter products and RINEX observation files used in this study are publicly available through the IGS Data Center at Wuhan University at ftp://igs.gnsswhu.cn/pub/gps/ (accessed on 9 November 2026). The SLR normal-point observations are publicly available from the EUROLAS Data Center operated by Deutsches Geodätisches Forschungsinstitut of the Technical University of Munich at ftp://edc.dgfi.tum.de/pub/slr/data/ (accessed on 9 November 2026).

Acknowledgments: The authors thank the IGS MGEX analysis centers for providing precise orbit and clock products and the ILRS for providing SLR observations.

Conflicts of Interest: The authors declare no conflicts of interest.

Abbreviations

The following abbreviations are used in this manuscript:

AC	Analysis center
ADEV	Allan deviation
BDS	BeiDou Navigation Satellite System
CAST	China Academy of Space Technology
CODE	Center for Orbit Determination in Europe
CoM	Center of mass
CSNO	China Satellite Navigation Office
ECOM	Empirical CODE Orbit Model
GEO	Geostationary Earth orbit
GFZ	German Research Centre for Geosciences
GLONASS	Global Navigation Satellite System
GNSS	Global Navigation Satellite System
GPS	Global Positioning System
IAC	Information and Analysis Center for Positioning, Navigation and Timing
IERS	International Earth Rotation and Reference Systems Service
IGS	International GNSS Service
IGSO	Inclined geosynchronous orbit
ILRS	International Laser Ranging Service
LRA	Laser retroreflector array
MAD	Median absolute deviation
MEO	Medium Earth orbit
MGEX	Multi-GNSS Experiment
PCO	Phase center offset
PCV	Phase center variation
PDOP	Position dilution of precision
POD	Precise orbit determination
PPP	Precise point positioning
PRN	Pseudo-random noise
RAC	Radial, along-track, and cross-track
RINEX	Receiver Independent Exchange Format
RMS	Root mean square
SECM	Shanghai Engineering Center for Microsatellites
SLR	Satellite Laser Ranging
SRP	Solar radiation pressure
STD	Standard deviation
SVN	Space vehicle number
WHU	Wuhan University

References

1. Yang, Y.; Gao, W.; Guo, S.; Mao, Y.; Yang, Y. Introduction to BeiDou-3 navigation satellite system. *Navigation* **2019**, *66*, 7–18. [CrossRef]
2. Teunissen, P.J.G.; Montenbruck, O. (Eds.) *Springer Handbook of Global Navigation Satellite Systems*; Springer International Publishing: Cham, Switzerland, 2017. [CrossRef]
3. Zhao, Q.; Guo, J.; Wang, C.; Lyu, Y.; Xu, X.; Yang, C.; Li, J. Precise orbit determination for BDS satellites. *Satell. Navig.* **2022**, *3*, 2. [CrossRef]

4. Montenbruck, O.; Steigenberger, P.; Prange, L.; Deng, Z.; Zhao, Q.; Perosanz, F.; Romero, I.; Noll, C.; Stürze, A.; Weber, G.; et al. The Multi-GNSS Experiment (MGEX) of the International GNSS Service (IGS)—Achievements, prospects and challenges. *Adv. Space Res.* **2017**, *59*, 1671–1697. [CrossRef]
5. Steigenberger, P.; Montenbruck, O. Consistency of MGEX orbit and clock products. *Engineering* **2020**, *6*, 898–903. [CrossRef]
6. Guo, F.; Li, X.; Zhang, X.; Wang, J. Assessment of precise orbit and clock products for Galileo, BeiDou, and QZSS from IGS Multi-GNSS Experiment (MGEX). *GPS Solut.* **2017**, *21*, 279–290. [CrossRef]
7. Li, X.; Zhu, Y.; Zheng, K.; Yuan, Y.; Liu, G.; Xiong, Y. Precise orbit and clock products of Galileo, BDS and QZSS from MGEX since 2018: Comparison and PPP validation. *Remote Sens.* **2020**, *12*, 1415. [CrossRef]
8. Shen, P.; Cheng, F.; Lu, X.; Xiao, X.; Ge, Y. An investigation of precise orbit and clock products for BDS-3 from different analysis centers. *Sensors* **2021**, *21*, 1596. [CrossRef] [PubMed]
9. Gu, S.; Mao, F.; Gong, X.; Lou, Y.; Xu, X.; Zhou, Y. Evaluation of BDS-2 and BDS-3 satellite atomic clock products and their effects on positioning. *Remote Sens.* **2021**, *13*, 5041. [CrossRef]
10. Geng, T.; Jiang, R.; Lv, Y.; Xie, X. Analysis of BDS-3 onboard clocks based on GFZ precise clock products. *Remote Sens.* **2022**, *14*, 1389. [CrossRef]
11. Steigenberger, P.; Deng, Z.; Guo, J.; Prange, L.; Song, S.; Montenbruck, O. BeiDou-3 orbit and clock quality of the IGS Multi-GNSS Pilot Project. *Adv. Space Res.* **2023**, *71*, 355–368. [CrossRef]
12. Chen, X.; Ge, M.; Liu, Y.; He, L.; Schuh, H. Adapting empirical solar radiation pressure model for BDS-3 medium Earth orbit satellites. *GPS Solut.* **2023**, *27*, 183. [CrossRef]
13. Guo, J.; Wang, C.; Chen, G.; Xu, X.; Zhao, Q. BDS-3 precise orbit and clock solution at Wuhan University: Status and improvement. *J. Geod.* **2023**, *97*, 15. [CrossRef]
14. Zajdel, R.; Nowak, A.; Sośnica, K. Satellite laser ranging to BeiDou-3 satellites: Initial performance and contribution to orbit model improvement. *GPS Solut.* **2024**, *28*, 100. [CrossRef]
15. Xie, S.; Huang, G.; Wang, L.; Lai, W.; She, H. Study of the SRP model for BDS-3 satellites SVN C223 and C222 to mitigate SLR residual anomalies. *Satell. Navig.* **2025**, *6*, 13. [CrossRef]
16. International GNSS Service. MGEX Data and Products: Precise Orbit and Clock Products. Available online: https://igs.org/mgex/data-products/#orbit_clock (accessed on 19 July 2026).
17. Zhao, Q.; Li, M. Wuhan University Data Center: Technical Report 2023. In *IGS Technical Report 2023*; IGS Central Bureau: Pasadena, CA, USA; Bern Open Publishing, University of Bern: Bern, Switzerland, 2024; pp. 175–178. Available online: https://files.igs.org/pub/resource/technical_reports/2023_techreport.pdf (accessed on 20 October 2026).
18. China Satellite Navigation Office. *BeiDou Navigation Satellite System Open Service Performance Standard*, Version 3.0; China Satellite Navigation Office: Beijing, China, 2021. Available online: http://en.beidou.gov.cn/SYSTEMS/Officialdocument/202110/P020211014595952404052.pdf (accessed on 20 October 2026).
19. International GNSS Service. MGEX Constellations: BeiDou. Available online: https://igs.org/mgex/constellations/#beidou (accessed on 19 July 2026).
20. International GNSS Service. Antenna Working Group. Available online: https://igs.org/wg/antenna/ (accessed on 20 October 2026).
21. Dach, R.; Lutz, S.; Walser, P.; Fridez, P. (Eds.) *Bernese GNSS Software Version 5.2: User Manual*; Astronomical Institute, University of Bern, Bern Open Publishing: Bern, Switzerland, 2015. [CrossRef]
22. German Research Centre for Geosciences (GFZ). GFZ Analysis Strategy Summary. Available online: https://files.igs.org/pub/center/analysis/GFZ0MGXFIN.acn (accessed on 20 October 2026).
23. Information and Analysis Center (IAC). IAC Analysis Strategy Summary. Available online: https://files.igs.org/pub/center/analysis/IAC0MGXFIN.acn (accessed on 20 October 2026).
24. Liu, J.; Ge, M. PANDA software and its preliminary result of positioning and orbit determination. *Wuhan Univ. J. Nat. Sci.* **2003**, *8*, 603–609. [CrossRef]
25. Dilssner, F. A Note on the Yaw Attitude Modeling of BeiDou IGSO-6; Technical Note, 20 November 2017. Available online: https://igs.org/mgex/constellations/ (accessed on 19 July 2026).
26. Wang, C.; Guo, J.; Zhao, Q.; Liu, J. Yaw attitude modeling for BeiDou I06 and BeiDou-3 satellites. *GPS Solut.* **2018**, *22*, 117. [CrossRef]
27. Zhao, Q.; Wang, C.; Guo, J.; Wang, B.; Liu, J. Precise orbit and clock determination for BeiDou-3 experimental satellites with yaw attitude analysis. *GPS Solut.* **2018**, *22*, 4. [CrossRef]
28. Lin, X.; Lin, B.; Liu, Y.; Xiong, S.; Bai, T. Satellite geometry and attitude mode of BDS-3 MEO satellites developed by SECM. In Proceedings of the 31st International Technical Meeting of the Satellite Division of the Institute of Navigation (ION GNSS+ 2018), Miami, FL, USA, 24–28 September 2018; pp. 1268–1289. [CrossRef]

29. China Satellite Navigation Office. *Definitions and Descriptions of BDS/GNSS Satellite Parameters for High Precision Applications (BD 420025-2019)*; China Satellite Navigation Office: Beijing, China, 2019. Available online: https://ilrs.cddis.eosdis.nasa.gov/docs/2019/BeiDou_MetaData_191201.cn.en.pdf (accessed on 19 July 2026).
30. Wang, C. Solar Radiation Pressure Modelling for BeiDou Navigation Satellites. Ph.D. Thesis, Wuhan University, Wuhan, China, 2019.
31. Yan, X.; Liu, C.; Huang, G.; Zhang, Q.; Wang, L.; Qin, Z.; Xie, S. A priori solar radiation pressure model for BeiDou-3 MEO satellites. *Remote Sens.* **2019**, *11*, 1605. [CrossRef]
32. Arnold, D.; Meindl, M.; Beutler, G.; Dach, R.; Schaer, S.; Lutz, S.; Prange, L.; Sośnica, K.; Mervart, L.; Jäggi, A. CODE's new solar radiation pressure model for GNSS orbit determination. *J. Geod.* **2015**, *89*, 775–791. [CrossRef]
33. Beutler, G.; Brockmann, E.; Gurtner, W.; Hugentobler, U.; Mervart, L.; Rothacher, M.; Verdun, A. Extended orbit modeling techniques at the CODE processing center of the International GPS Service for Geodynamics (IGS): Theory and initial results. *Manuscr. Geod.* **1994**, *19*, 367–386. [CrossRef]
34. Springer, T.A.; Beutler, G.; Rothacher, M. A new solar radiation pressure model for GPS satellites. *GPS Solut.* **1999**, *2*, 50–62. [CrossRef]
35. Rousseeuw, P.J.; Croux, C. Alternatives to the median absolute deviation. *J. Am. Stat. Assoc.* **1993**, *88*, 1273–1283. [CrossRef]
36. Rudenko, S.; Dettmering, D.; Lemoine, J.-M.; Bloßfeld, M.; Zeitlhöfler, J. Impact of Earth's Mean Time-Variable Gravity Field Models on Precise Orbits of Altimetry Satellites. *Surv. Geophys.* **2026**, *47*, 1169–1202. [CrossRef]
37. Yuan, Y.; Li, X.; Zheng, H.; Gao, C.; Yao, X. Incorporating Satellite Laser Ranging observations into BDS analysis: From the perspectives of orbit validation, precise orbit determination, and geodetic parameters estimation. *J. Geod.* **2025**, *99*, 13. [CrossRef]
38. Strugarek, D.; Sośnica, K.; Arnold, D.; Jäggi, A.; Zajdel, R.; Bury, G. Satellite laser ranging to GNSS-based Swarm orbits with handling of systematic errors. *GPS Solut.* **2022**, *26*, 104. [CrossRef]
39. Urschl, C.; Beutler, G.; Gurtner, W.; Hugentobler, U.; Schaer, S. Contribution of SLR tracking data to GNSS orbit determination. *Adv. Space Res.* **2007**, *39*, 1515–1523. [CrossRef]
40. Zajdel, R.; Sośnica, K.; Bury, G. A New Online Service for the Validation of Multi-GNSS Orbits Using SLR. *Remote Sens.* **2017**, *9*, 1049. [CrossRef]
41. Sośnica, K.; Zajdel, R.; Bury, G.; Bosy, J.; Moore, M.; Masoumi, S. Quality assessment of experimental IGS multi-GNSS combined orbits. *GPS Solut.* **2020**, *24*, 54. [CrossRef]
42. Li, X.; Liu, C.; Yuan, Y.; Zhang, K. Current Status and Challenges of BDS Satellite Precise Orbit Products: From a View of Independent SLR Validation. *Remote Sens.* **2023**, *15*, 2782. [CrossRef]
43. International Laser Ranging Service. COMPASS/BeiDou Mission Parameters. Available online: https://ilrs.gsfc.nasa.gov/missions/satellite_missions/current_missions/cmg8_general.html (accessed on 19 July 2026).
44. Li, R.; Wang, C.; Ma, H.; Zhou, Y.; Tang, C.; Wu, Z.; Yang, G.; Zhang, X. SLR validation and evaluation of BDS-3 MEO satellite precise orbits. *Remote Sens.* **2024**, *16*, 2016. [CrossRef]
45. International Laser Ranging Service. SLR Station Coordinates: SLRF2020, Version 2026.02.05. Available online: https://ilrs.gsfc.nasa.gov/network/site_information/index.html (accessed on 18 October 2026).
46. International Laser Ranging Service. COMPASS/BeiDou Array Offset Information: LRA–CoM Offsets from CSNO TARC. Available online: https://ilrs.gsfc.nasa.gov/missions/satellite_missions/current_missions/cms2_com.html (accessed on 18 October 2026).
47. Mendes, V.B.; Pavlis, E.C. High-accuracy zenith delay prediction at optical wavelengths. *Geophys. Res. Lett.* **2004**, *31*, L14602. [CrossRef]
48. Lyard, F.H.; Allain, D.J.; Cancet, M.; Carrère, L.; Picot, N. FES2014 global ocean tide atlas: Design and performance. *Ocean Sci.* **2021**, *17*, 615–649. [CrossRef]
49. Mathews, P.M.; Dehant, V.; Gipson, J.M. Tidal station displacements. *J. Geophys. Res. Solid Earth* **1997**, *102*, 20469–20477. [CrossRef]
50. Petit, G.; Luzum, B. (Eds.) *IERS Conventions (2010)*; IERS Technical Note No. 36; Verlag des Bundesamts für Kartographie und Geodäsie: Frankfurt am Main, Germany, 2010.
51. Allan, D.W. Statistics of atomic frequency standards. *Proc. IEEE* **1966**, *54*, 221–230. [CrossRef]
52. Riley, W.J. *Handbook of Frequency Stability Analysis*; NIST Special Publication 1065; National Institute of Standards and Technology: Boulder, CO, USA, 2008. [CrossRef]
53. Zumberge, J.F.; Heflin, M.B.; Jefferson, D.C.; Watkins, M.M.; Webb, F.H. Precise point positioning for the efficient and robust analysis of GPS data from large networks. *J. Geophys. Res. Solid Earth* **1997**, *102*, 5005–5017. [CrossRef]
54. Wu, J.T.; Wu, S.C.; Hajj, G.A.; Bertiger, W.I.; Lichten, S.M. Effects of antenna orientation on GPS carrier phase. *Manuscr. Geod.* **1993**, *18*, 91–98. [CrossRef]
55. Kouba, J. A Guide to Using International GNSS Service (IGS) Products. Updated September 2015. Available online: https://files.igs.org/pub/resource/pubs/UsingIGSProductsVer21_cor.pdf (accessed on 20 October 2026).

56. Landskron, D.; Böhm, J. VMF3/GPT3: Refined discrete and empirical troposphere mapping functions. *J. Geod.* **2018**, *92*, 349–360. [CrossRef] [PubMed]
57. Yang, C.; Guo, J.; Zhao, Q. Yaw attitudes for BDS-3 IGSO and MEO satellites: Estimation, validation and modeling with intersatellite link observations. *J. Geod.* **2023**, *97*, 6. [CrossRef]

Disclaimer/Publisher's Note: The statements, opinions and data contained in all publications are solely those of the individual author(s) and contributor(s) and not of MDPI and/or the editor(s). MDPI and/or the editor(s) disclaim responsibility for any injury to people or property resulting from any ideas, methods, instructions or products referred to in the content.